JOURNAL OF APPLIED ELECTROCHEMISTRY **28** (1998) 843–853

Photocatalytic degradation rate of oxalic acid on the semiconductive layer of *n*-TiO_2 particles in the batch mode plate reactor Part I: Mass transfer limits

J. KULAS, I. ROUŠAR†, J. KRÝSA

Institute of Chemical Technology, Department of Inorganic Technology, Technická 5, CZ-166 28 Prague 6, Czech Republic

J. JIRKOVSKÝ

J. Heyrovsky Institute of Physical Chemistry, Academy of Sciences, Dolejškova 3, CZ-182 23 Prague 8, Czech Republic

Received 17 April 1997; revised 11 September 1997

Organic compounds dissolved in water can be decomposed on a layer of *n*-TiO_2 particles irradiated by u.v. light, which generates holes and electrons in the TiO_2 material. Dissolved oxygen was used as electron scavenger and holes reacted with water to give OH radicals. The rate of degradation of the dissolved organic compounds by OH radicals is limited by the transfer of either oxygen or of the organic compounds to the surface of *n*-TiO_2 particles. The consequence of these limits is that, in the batch mode reactor with recirculation of the liquid, the dependence of the concentration of an organic compound on time has either a linear or an exponential form. Experiments with decomposition of oxalic acid in aqueous solutions using a plate reactor (60 cm × 120 cm) confirmed the analysis. Equations for evaluation of the mass transfer coefficient of the dissolved species to the surface of the plate reactor with a moving liquid film were developed for the case of the thickness of the Nernst diffusion layer being thinner than the thickness of the liquid. The experimentally obtained decomposition rate of oxalic acid was about 60 to 80% of the theoretical decomposition rate limited by oxygen flux through the film of a moving liquid. The present theory neglects the diffusion of oxygen into the porous layer of *n*-TiO_2.

Keywords: *mass transfer*, *n-TiO₂*, *oxalic acid*, *photocatalytic degradation*

List of symbols

A	active surface of the reactor plate (cm^2)
A_P	cross-sectional area of the Petri dish (cm^2)
c	concentration ($mol\,cm^{-3}$)
c_1	velocity of the light ($cm\,s^{-1}$)
D	diffusion coefficient ($cm^2\,s^{-1}$)
d_e	equivalent diameter (cm)
g	gravitational intensity ($N\,kg^{-1}$)
h	Planck constant (J s)
I	intensity of u.v. light ($W\,cm^{-2}$)
J	flux density ($mol\,cm^{-2}\,s^{-1}$) or ($einstein\,cm^{-2}\,s^{-1}$)
k	constant (Equations 50 and 51)
k_L	mass transfer coefficient ($cm\,s^{-1}$)
L	length of the reactor plate (cm)
n	molar amount (mol)
N_A	Avogadro constant (mol^{-1})
$(org)_{ads}$	number of adsorbed organic molecules
Q	flow rate ($cm^3\,s^{-1}$)
Re	Reynolds number
Sc	Schmidt number
Sh	Sherwood number
S_0	number of active surface sites
v	velocity of the film ($cm\,s^{-1}$)
V	volume (cm^3)
V_P	volume of oxalic acid in the Petri dish (cm^3)
w	width of the reactor plate (cm)

Greek symbols

α	inclination angle of the reactor plate to the horizontal
δ	thickness (cm)
λ	wavelength of the light (cm)
ν	kinematic viscosity or stoichiometric coefficient

† deceased.

0021-891X

τ time (s)
Θ the coverage of the active surface sites

Subscripts
$(COOH)_2$ oxalic acid
f liquid film
hv radiation quantum
i species
lim limiting
N Nernst
O_2 oxygen
org organic compound
r reactor
y direction

Superscripts
0 bulk
s surface
i initial

1. Introduction

Advanced oxidative processes such as semiconductor photocatalysis [1] are intended to be both supplementary and complementary to some of the more conventional approaches to the destruction or transformation of hazardous chemical wastes such as the adsorption of the pollutant species onto activated carbon [2], oxidation with hydrogen peroxide or chlorine [3–5], high-temperature incineration, amended activated sludge digestion, anaerobic digestion and other conventional physicochemical treatments [6–10].

Over the last 10 years the scientific and engineering interest in the application of semiconductor photocatalysis has grown exponentially [11]. Heterogeneous photocatalytic oxidation of organic substrates dissolved in water in the presence of oxygen can occur on the semiconductive layer of the photocatalyst (mostly titanium dioxide). In contradistinction to homogenous photocatalysis, this method is especially advantageous in terms of its costs, because it can work with the ultraviolet band from the solar spectrum.

The heterogeneous photocatalytical system consists of semiconductive particles, which act as a photocatalyst in contact with the reaction medium (liquid or gaseous). The simplified scheme of the photocatalysis is shown in Fig. 1; this represents a semiconductive particle, spherical in shape, with indication of the positions of the valence and conduction energy bands. In most cases A stands for oxygen and D for water. Thus $A^{\cdot-}$ is O_2^- and $D^{\cdot}$ is $OH^{\cdot}$.

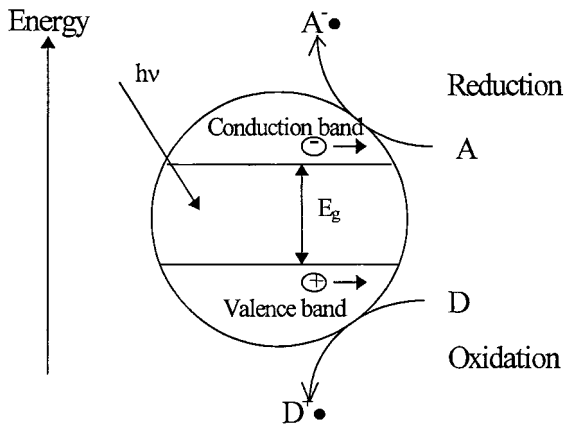

Fig. 1. Graphical representation of the formation of holes and electrons from photons with energy higher then the energy of the gap between the conduction and valence band. D reacts with holes, A reacts with electrons.

Irradiation with photons, which have their energy, *hv*, greater than the bandgap energy, can generate in the photocatalyst charge carrier pairs, holes and electrons:

$$TiO_2 \xrightarrow{hv} h^+ + e^- \quad (1)$$

After the charge carriers are transported to the surface, they react with molecules by a redox reaction, when the redox potentials of molecules of an acceptor and of a donor happen to lie within the bandgap. However, before the electrons and holes reach the surface, there is a significant chance of recombination, and this is an important source of inefficiency in a system employing semiconductor catalysts for photochemical conversion of light [12].

The position of the valence and conduction energy bands determines whether the transfer of the photogenerated charge carrier is thermodynamically possible by the given redox system. A special characteristic of semiconductive metallic oxides is, that their holes have an extremely high oxidative potential. This enables the one electron oxidation of water in which the strong oxidative $OH^{\cdot}$ radicals are generated [11].

$$H_2O_{ads} + h^+ \rightarrow OH^{\cdot}_{ads} + H^+ \quad (2)$$

These radicals can react with many organic molecules and thus they contribute in a high degree to their photocatalytic degradation.

The dissolved oxygen is generally used as the electron acceptor

$$O_2 + e^- \rightarrow O_2^{\cdot -} \quad (3)$$

In acidic media (pH = 3) the superoxide radical anion protonates to give hydroperoxide radical $HO_2^{\cdot}$ [13]

$$2\,O_2^{\cdot -} + 2H^+ \rightarrow 2\,HO_2^{\cdot} \quad (4)$$

From hydroperoxide radical the hydrogen peroxide and oxygen can originate

$$2\,HO_2^{\cdot} \rightarrow H_2O_2 + O_2 \quad (5)$$

The photocatalytic reduction of hydrogen peroxide then leads to the production of hydroxyl radicals.

$$H_2O_2 + e^- \rightarrow OH^{\cdot} + OH^- \quad (6)$$

Thus the strong reductively acting particle (e^-) in Reaction 1 is changed via Reactions 3–6 to the strong oxidatively acting particle ($OH^{\cdot}$), so that it can ac-

celerate the decomposition reaction by hydrogen peroxide as the oxidizing agent. On the other hand the hydrogen peroxide can react with a hole and thus the decomposition rate of the organic compound can be decreased [14].

Titanium dioxide crystallizes in three polymorphic systems, brookite, rutile and anatase, and is available only as an n-semiconductor. Anatase is more photoactive than rutile. The bandgap width for rutile is 3 eV and for anatase 3.2 eV. The bandgap energy determines the wavelength threshold, from which the semiconductor can absorb light. Therefore, for induction of photocatalytic reaction, titanium dioxide can absorb only u.v.-light with wavelengths shorter than 413 nm (rutile), or 388 nm (anatase). The u.v.-share of the sun spectrum with wavelengths lower than 400 nm corresponds to only 5% of the total irradiated sun energy [15].

The use of TiO_2 catalyst in the form of a slurry has the great advantage of having good mass transfer characteristics. When the slurry consists of very fine particles, it requires a very long settlement time for the catalyst to be removed from the purified water, or fine filters must be employed. Recently, attention has been turned to the application of immobilized catalysts [16–18] in the form of TiO_2 powder attached to the sides of the tray, which constitutes the main part of a flow-through reactor. The use of a fixed TiO_2 film leads to some mass-transfer problems which also arise when a suspension is used. If the film is too thick, most of the holes are generated too deep in the bulk of the semiconductor and never reach the surface. If the film is too thin, only part of the incidental light will be absorbed.

During heterogeneous catalysis involving simultaneous reactions at a catalytic surface, the apparent rate of reaction (the measured rate) can be dominated by surface kinetics, liquid film transport kinetics or by a combination of both. The rate of photocatalytic reaction involving TiO_2 particles which are uniformly distributed as freely suspended particles in the solution is completely controlled by the intrinsic reaction rate on the catalyst surface. In contrast, experiments involving active particles coated on tube surfaces or large glass beds may frequently have apparent kinetics that are influenced by mass transfer [19] as indicated by a measured influence of liquid flow rate on the apparent rate coefficient. Since only the mass transfer coefficient, k_m, is influenced by fluid velocity, an influence by the latter on the flow rate is an unambiguous result [20–22].

The aim of this paper is a chemical engineering description of three limiting cases connected with the mass transfer flux and photon flux to the surface of n-TiO_2 particles fixed on the reactor plate. The existence of these limiting cases was confirmed by the study of photocatalytic degradation of a model substance – oxalic acid in a liquid film which circulates over the semiconductive layer of titanium dioxide particles fixed onto a glass plate. The plate reactor was used in a batch mode.

2. Theory

The consumption of photons per mole of electron scavenger and per molecule of organic compound forms the background of the calculation. The development of equations for mass transfer coefficients then permits the calculation of the limiting flux density.

2.1. *Consumption of photons per mole of electron scavenger (oxygen)*

Let us suggest, that oxygen and hydrogen peroxide may react with electrons formed from a photon. Then Reactions 1–6 proceed on the surface of n-TiO_2 anatase. The reduction of oxygen due to Reactions 3–6 may be summarized as

$$O_2 + 3e^- + 3H^+ \rightarrow OH\cdot + H_2O \qquad (7)$$

It is assumed that Reactions 1, 2 and 7 proceed at the same rate. The generation of OH· is due to the reactions of the holes with water (2) and of electrons with oxygen (7). The overall reaction for formation of OH· can be written as:

$$O_2 + 3h\nu + 2\,H_2O \rightarrow 4\,OH\cdot \qquad (8)$$

Another possibility is the reduction of H_2O_2 by electrons to OH^- which gives

$$H_2O_2 + 2e^- \rightarrow 2OH^- \qquad (9)$$

Combining Reactions 3–6 and 9 gives

$$O_2 + 2\,H_2O + 4e^- \rightarrow 4\,OH^- \qquad (10)$$

From the comparison of Equations 7 and 10 it follows that the consumption of one oxygen molecule is connected with the consumption of 3 or 4 electrons.

2.2. *Consumption of a model compound and oxygen*

Oxalic acid will be used as the model compound. Starting with OH· produced by Reaction 8, the oxidation of the oxalic acid may be written as

$$2\,(COOH)_2 + 4\,OH\cdot \rightarrow 4\,CO_2 + 4\,H_2O \qquad (11)$$

or in a more condensed form

$$2\,(COOH)_2 + (O_2 + 3h\nu) \rightarrow 4\,CO_2 + 2\,H_2O \qquad (12)$$

In the oxidation path of oxalic acid via Reactions 1, 2 and 10 four photons per molecule of oxygen are consumed:

$$2\,(COOH)_2 + (O_2 + 4h\nu) \rightarrow 4\,CO_2 + 2\,H_2O \qquad (13)$$

Equations 12 and 13 describe the oxidation of oxalic acid via different mechanisms and with a different consumption of photons (3/2, 4/2) per molecule of oxalic acid. On the other hand, the consumption of oxygen molecules (1/2) per molecule of oxalic acid is the same for any of the aformentioned mechanisms. The stoichiometric coefficient for $h\nu$ in Equations 12 and 13 will be denoted as $\nu_{h\nu}$.

2.3. *Balance equations for a plate reactor in batch mode*

The rate of oxidation of an organic compound in a batch mode reactor with volume of liquid V_r and a photocatalytically active surface of a plate (A) of width w and length $L(A = wL)$ can be expressed in differential form as

$$-\left|J_{org}\right| = \frac{V_r}{A}\frac{dc_{org}}{d\tau} \tag{14}$$

It is suggested that the volume of liquid covering the reactor plate, V_p, is negligible in comparison with the total volume of liquid, V_r. The liquid is well mixed in the reservoir and recirculates over the plate at a volumetric flow rate Q [$cm^3\,s^{-1}$]. The concentration changes of the organic compound in the liquid film along the reactor plate are negligible in comparison with the bulk concentration of that compound (see Section 4.2.1. where the decrease in oxalic acid in the flowing liquid film is calculated).

The molar flux of photons used for the decomposition of the organic compound follows from the stoichiometry of the Reactions 12 or 13:

$$J_{h\nu} = \frac{\nu_{h\nu}}{\nu_{org}}\left|J_{org}\right| \tag{15}$$

Similarly, for the flux density of oxygen Equation 16 is valid:

$$\left|J_{O_2}\right| = \frac{1}{\nu_{org}}\left|J_{org}\right| \tag{16}$$

The limiting flux density of species 'i' is defined for the case, when the concentration of species 'i' (oxygen or the organic compound) at the surface of the n-TiO_2 layer is just zero. Introducing a limiting flux density the following classification of limiting cases is possible. There are three different limiting cases due to the coupling of Reactions 1–3 and 12 or 13. The limiting flux densities for oxygen, the organic compound and photons may fulfil one of the following conditions:

$$\text{(i)}\ \left|J_{O_2,lim}\right| \ll \frac{J_{photons}}{\nu_{h\nu}} \approx \frac{1}{\nu_{org}}\left|J_{org,lim}\right| \tag{17}$$

$$\text{(ii)}\ \frac{1}{\nu_{org}}\cdot\left|J_{org,lim}\right| \ll \left|J_{O_2,lim}\right| \approx \frac{J_{photons}}{\nu_{h\nu}} \tag{18}$$

$$\text{(iii)}\ \frac{J_{photons}}{\nu_{h\nu}} \ll \left|J_{O_2,lim}\right| \approx \frac{1}{\nu_{org}}\left|J_{org,lim}\right| \tag{19}$$

The following equation gives the flux density of the species 'i' (e.g., a dissolved molecular oxygen or the organic compound) to the surface of the n-TiO_2 layer:

$$J_i = -D_i\frac{\left(c_i^o - c_i^s\right)}{\delta_{N,i}} \tag{20}$$

The mass transfer coefficient $k_{L,i}$ may be introduced as

$$k_{L,i} = \frac{D_i}{\delta_{N,i}} \tag{21}$$

Case (i) describes the situation, when the flux density of photons is high and comparable with the limiting flux density of the organic compound to the surface of the plate covered with TiO_2. The flux density of oxygen is limiting when $c_{O_2}^s = 0$.

The concentration of the organic compound at the surface of TiO_2 (c_{org}^s) is high and close to the bulk concentration (c_{org}^0):

$$-\frac{dc_{org}^0}{d\tau} = \frac{A}{V_r}\left|J_{O_2,lim}\right|\nu_{org} \tag{22}$$

The flux density of oxygen $J_{O_2,lim}$ does not depend on c_{org}. Integration of Equation 22 leads to

$$c_{org}^0(\tau) = c_{org}^0(\tau = 0) - \frac{A}{V_r}\left|J_{O_2,lim}\right|\nu_{org}\tau \tag{23}$$

where

$$J_{O_2,lim} = -D_{O_2}\frac{c_{O_2}^0}{\delta_{N,O_2}} \tag{24}$$

In case (i) the concentration of the organic compound in the liquid of volume V_r decreases linearly with time.

Case (ii) is valid for a very low bulk concentration of the organic compound. Due to the excess of oxygen and photons the surface concentration of the organic compound (c_{org}^s) is zero. Then $J_{org,lim}$ may be expressed as

$$J_{org,lim} = -D_{org}\frac{c_{org}^0}{\delta_{N,org}} \tag{25}$$

In this case

$$-\frac{dc_{org}^0}{d\tau} = \frac{A}{V_r}\left|J_{org,lim}\right| \tag{26}$$

or using Equation 27

$$-\frac{dc_{org}^0}{d\tau} = \frac{A}{V_r}\frac{D_{org}c_{org}^0}{\delta_{N,org}} \tag{27}$$

which, after integration, gives

$$c_{org}^0(\tau) = c_{org}^0(\tau = 0)\exp\left[-\frac{A}{V_r}\frac{D_{org}}{\delta_{N,org}}\tau\right] \tag{28}$$

In Equations 24 and 28 the unknown parameter is the thickness of the Nernst diffusion layer, δ_N.

2.4. *Calculation of Nernst diffusion layer thickness and mass transfer coefficient*

For the case of laminar liquid film flow on the surface of a reactor plate an approximate solution [23] was developed based on the suggestion of a constant thickness of the liquid film δ_f over the plate length L:

$$\delta_f = \left(\frac{3\nu^2}{g\,\sin\alpha}\right)^{1/3}(Re_f)^{1/3} \tag{29}$$

Re_f is the film Reynolds number given by

$$Re_f = \frac{Q}{w\nu} \tag{30}$$

The validity of Equation 29 was verified by Goodridge [24].

The average velocity in the film $\overline{v_f}$ can be calculated as

$$\overline{v_f} = \frac{Q}{w\delta_f} \tag{31}$$

In [23] it was suggested, that the velocity in the film has a parabolic profile with a maximum velocity at $x = \delta_f$

$$v_y = 6\overline{v_f}\left(\frac{x}{2\delta_f} - \left(\frac{x}{2\delta_f}\right)^2\right) \tag{32}$$

For this velocity profile it is possible to use the results obtained for mass transfer to the surface of a reactor plate for the case of a laminar flow in a rectangular duct [25]:

$$Sh = 1.85\left(\frac{d_e}{L} Re\, Sc\right)^{1/3} \Phi \tag{33}$$

where
$\Phi = 1$ for $w \gg \delta_f$ and

$$Sh = -\frac{J_i d_e}{D_i(c_i^0 - c_i^s)} \tag{34}$$

$$Re = \frac{\overline{v_f} d_e}{\nu} \tag{35}$$

$$Sc = \frac{\nu}{D_i} \tag{36}$$

$$d_e = 4\delta_f \tag{37}$$

and using Equations 29, 31 and 33 the average and local thickness (δ_N and $\delta_N(y)$) of the Nernst diffusion layer are given by

$$\delta_N = 1.095\left(\frac{1}{D_i^3 L^3}\frac{Q}{w}\left(\frac{g \sin\alpha}{\nu}\right)^2\right)^{-1/9} \tag{38}$$

$$\delta_N(y) = 1.644\left(\frac{1}{D_i^3 y^3}\frac{Q}{w}\left(\frac{g \sin\alpha}{\nu}\right)^2\right)^{-1/9} \tag{39}$$

For an average and a local mass transfer coefficient, k_L and $k_L(y)$, the following equations are valid:

$$k_L = 0.913\left(\frac{D_i^6}{L^3}\frac{Q}{w}\left(\frac{g \sin\alpha}{\nu}\right)^2\right)^{1/9} \tag{40}$$

$$k_L(y) = 0.608\left(\frac{D_i^6}{y^3}\frac{Q}{w}\left(\frac{g \sin\alpha}{\nu}\right)^2\right)^{1/9} \tag{41}$$

where y is calculated along the length of the plate. Equation 39 represents an approximation of the local Nernst diffusion layer for short plates. Thus the calculation of δ_N is reasonable when the local value of δ_N at the end of the plate $\delta_N(L) \ll \delta_f$ (see Fig. 2, in which the thickness of the film and the thickness of the average, δ_N, and local Nernst diffusion layer for $y = L, \delta_N(L)$, are given as a function of the film Reynolds number). The flow in the film is likely to be laminar, with no waves on the surface of the liquid film [26] and for a smooth plate surface. These two conditions are not fulfilled for real film reactors and

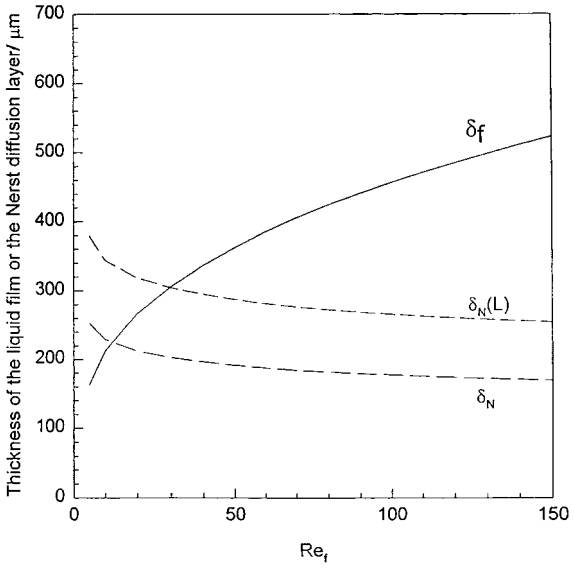

Fig. 2. Dependence of thickness of the flowing film, δ_f, thickness of the average, δ_N, and local Nernst diffusion layer for L, $\delta_{N,L}$, on the film Reynolds number using Equations 29, 30, 38 and 39 for $\nu = 0.01\,cm^2\,s^{-1}$, $\alpha = 10°$, $g = 981\,cm\,s^{-2}$, $D_i = 2.34 \times 10^{-5}\,cm^2\,s^{-1}$, $L = 120\,cm$.

Equations 38–41 only represent a good approximation of δ_N and k_L for real flow of a liquid film over a reactor plate covered with n-TiO_2 particles.

The average flux density of species 'i' can be calculated using the mass transfer coefficient $k_{L,i}$ as

$$J_i = k_{L,i}(c_i^0 - c_i^s) \tag{42}$$

Equation 42 permits the calculation of the flux density of oxygen or an organic compound to the surface of the reactor plate covered with n-TiO_2 particles. The layer of n-TiO_2 particles is porous and the oxygen or organic compound should diffuse into the TiO_2 layer. Thus Equations 38, 40 and 42, taking into account only convective-diffusion transport to the surface of the reactor plate, will overestimate the limiting flux densities of oxygen or the organic compound.

3. Experimental details

The main part of the plate solar reactor was formed by a rectangular polymethylmethacrylate tray with two troughs at either end (Fig. 3). The tray was dimensioned so that it could accommodate a glass plate plate of dimensions 60 cm × 120 cm × 0.5 cm. The whole assembly was supported by a rig with adjustable legs to allow adjustment of the inclination. The plate was inclined at an angle of ten degrees to the horizontal. Above the glass plate at a distance of 10.5 cm was an assembly of 10 ultraviolet sun bed bulbs (Osram Eversun L40W/79K). They were positioned at even intervals (12.5 cm from centre to centre) along the length of the plate.

The glass plate was coated with a layer of semiconductive titanium dioxide (P25, Degussa). The preparation of the TiO_2 layer was similar to that proposed by Bockelmann [14]. The glass plate was degreased and treated in 20% HNO_3 for six days.

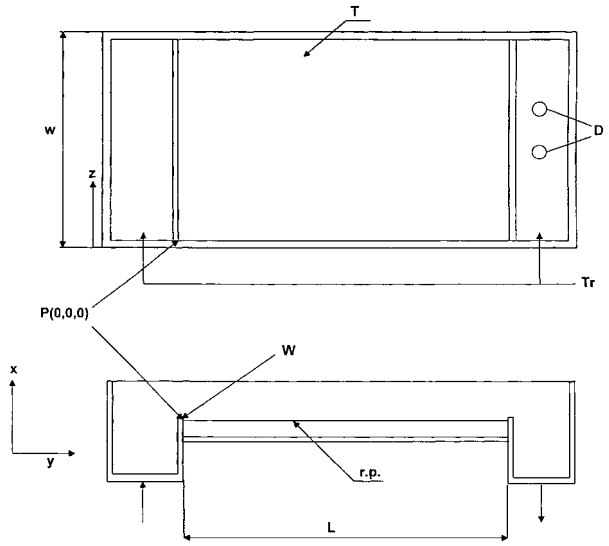

Fig. 3. Schematic representation of plate solar reactor with width w and length L. The solution enters the left trough, flows over the weir and leaves the reactor through drainage holes on the right side. P(0,0,0) is the origin; x-axis is oriented normal to the tray surface; y-axis is along the length (in the direction of fluid flow); z-axis is in the direction of the width of the plate; r.p. is the reactor plate ($w = 60\,\text{cm}, L = 120\,\text{cm}$); wr is the weir at the inlet of the fluid; T is the reactor tray; DH are the drainage holes and Tr is the trough.

Then it was placed into the container and a suspension of titanium dioxide in water (10 g TiO_2 dm^{-3}, pH 3) was poured onto the plate. The titanium dioxide was allowed to settle for six days and the water was then removed and the reactor plate was left to dry in air for three days. The dry titanium dioxide layer was then baked with stepwise increased temperature up to $300 \pm 10\,^{\circ}\text{C}$ for 2 h, followed by slow cooling for 12 h.

The polluted water was pumped from the fifteen litre holding tank (Fig. 4) using a 45 W, 220 V centrifugal pump to the highest trough which was filled until it overflowed. This overflow produced a film of solution flowing over the glass plate, secured in the tray. This solution was collected in the lower trough and returned to the holding tank.

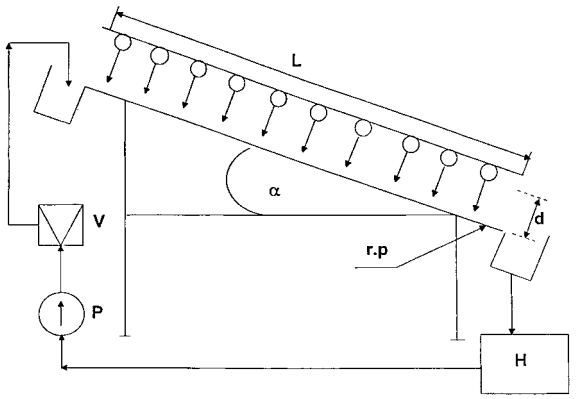

Fig. 4. Schematic representation of plate u.v.-reactor with the flow of the solution. The distance, d, between the sunbed bulbs and the plate covered with TiO_2 particles was 10.5 cm. Key: (H) holding tank (15 dm^3), (P) pump, (V) Venturi tube, UV= 10 pcs of sunbed bulbs, $d = 10.5$ cm (r.p.) reactor plate of width 60 cm and length 120 cm, (α) inclination angle 10°.

The flux of photons at the glass plate was determined by actinometry [27]. To determine the concentration of oxalic acid samples of the solution were taken and titrated with potassium permanganate solution. Using this analytical method, the possible intermediates (HCOH and HCOOH) are also determined and recalculated as the equivalent concentration of oxalic acid.

4. Results and discussion

4.1. *Photons flux at reactor plate surface*

To determine the flux of photons from the sunbed bulbs, uranyl oxalate actinometer was used. This was chosen because it degrades when exposed to light with wavelengths of between 208 and 436 nm [27]. Uranyl oxalate was prepared by reacting hydrated uranyl nitrate with an excess of hydrated oxalic acid (0.05 to 0.01 M ratio):

$$(\text{COOH})_2 \cdot 2\text{H}_2\text{O} + \text{UO}_2(\text{NO}_3) \cdot 6\text{H}_2\text{O} \rightarrow \text{UO}_2(\text{COO})_2 + 2\text{H}^+ + 2\text{NO}_3^- \quad (43)$$

When this solution, in a Petri dish, was exposed to u.v.-light, the excess oxalic acid was decomposed according to the following reactions:

$$\text{UO}_2^{2+} + (\text{COOH})_2 \xrightarrow{h\nu} \text{UO}_2^{2+} + \text{CO}_2 + \text{CO} + \text{H}_2\text{O} \quad (44)$$

$$\text{UO}_2^{2+} + (\text{COOH})_2 \xrightarrow{h\nu} \text{UO}_2^{2+} + \text{CO}_2 + \text{HCOOH} \quad (45)$$

$$\text{UO}_2^{2+} + (\text{COOH})_2 \xrightarrow{h\nu} \text{UO}_2\text{H}^+ + \text{H}^+ + 2\text{CO}_2 \quad (46)$$

Thus, by measuring the decrease in oxalate ions for given time intervals, it was possible to measure the flux of photons. The photon flux for the uranyl oxalate decomposition was calculated using Equation 47:

$$J_{\text{UO}_2} = \left(\frac{\text{d}c}{\text{d}\tau}\right)\frac{V_\text{p}}{A_\text{p}} \quad (47)$$

In the experiment, $c^\text{i} = 0.047\,87\,\text{mol}\,\text{cm}^{-3}$, $A_\text{p} = 103\,\text{cm}^2$, $V_\text{p} = 60\,\text{cm}^3$. The value of $(\text{d}c/\text{d}\tau)$ represents a slope evaluated by the least square method from a best fit linear average for three experiments (Fig. 5). This slope was $(2.22 \pm 0.24) \times 10^{-4}\,\text{s}^{-1}$. Using Equation 47 the molar flux of photons used for uranyl oxalate decomposition was calculated as $(6.197 \pm 0.67) \times 10^{-9}$ einstein $\text{cm}^{-2}\,\text{s}^{-1}$.

From the literature [27] the quantum yield for a uranyl oxalate actinometer $\Phi = 0.55$ is given for wavelengths between 240 and 440 nm. Using this value of Φ the flux of photons was calculated as J_{UO_2}/Φ, giving $J_{h\nu} = (1.13 \pm 0.11) \times 10^{-8}$ einstein $\text{cm}^{-2}\,\text{s}^{-1}$.

4.2. *Degradation of oxalic acid*

At the plate reactor the experiments with an oxalic acid solution circulated over the glass plate covered with titanium dioxide and a blank experiment with a

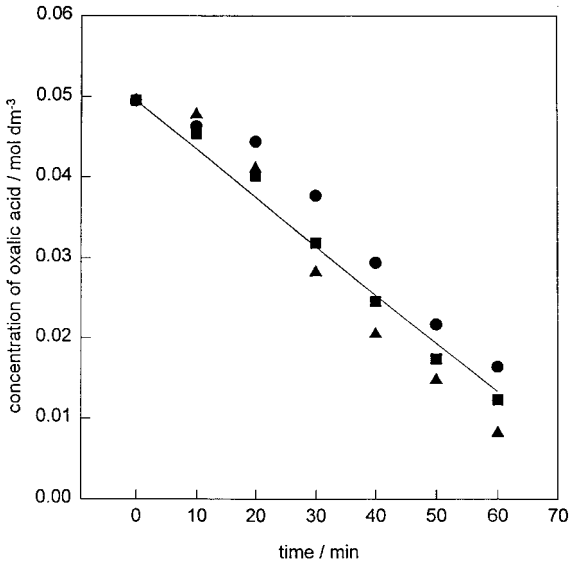

Fig. 5. Time decay of concentration of oxalic acid with UO_2 catalyst during actinometric measurement using a Petri dish.

plane glass plate were carried out. The results of these experiments are shown in Fig. 6. When the plain glass was used, the concentration of oxalic acid did not change during the irradiation of the flowing film. This means, that the photolytic degradation of oxalic acid by u.v.-light is negligible. The oxalic acid absorbs light with wavelengths lower than 230 nm and the sunbed bulbs used emit light with wavelengths 320–400 nm. When the oxalic acid solution was circulated over the glass plate covered with fixed *n*-TiO_2 particles and irradiated by u.v. light, the concentration of oxalic acid decreased linearly with time from $c = 0.01\ \text{mol dm}^{-3}$ to $c = 0.0001\ \text{mol dm}^{-3}$ in 9 h.

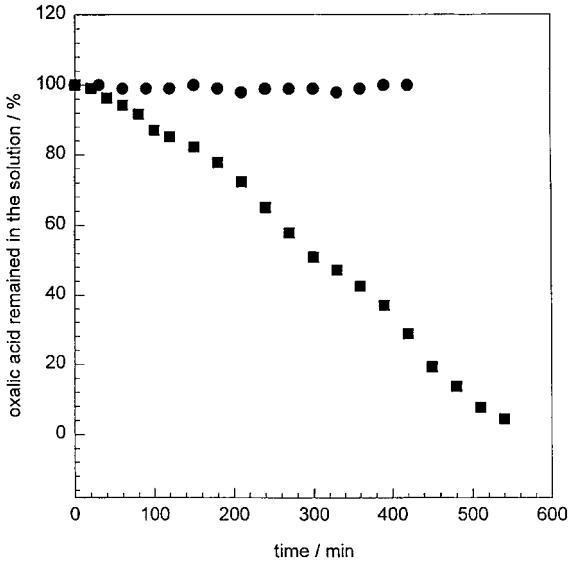

Fig. 6. Dependence of concentration of oxalic acid during the experiment using a plain glass plate (●) and the plate covered with TiO_2 particles (■). Experimental conditions: $w = 60$ cm, $L = 120$ cm, $Q = 3\ \text{dm}^{-3}\ \text{min}^{-1}$, initial concentration of oxalic acid $= 0.009\,37\ \text{mol dm}^{-3}$, $V_r = 15\ \text{dm}^3$, 10 sunbed bulbs at a distance 10.5 cm from the reactor plate, temperature (25 ± 1) °C, flux of photons 1.13×10^{-8} einstein $\text{cm}^{-2}\ \text{s}^{-1}$.

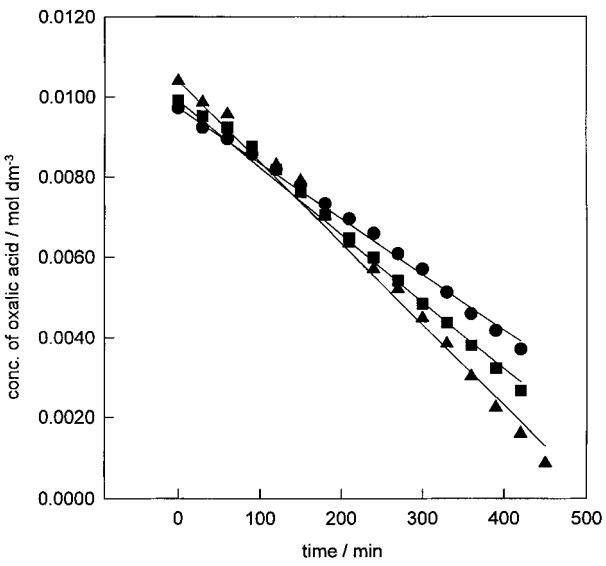

Fig. 7. Dependence of concentration of oxalic acid during the experiment using different flow-rate of the solution over the plate covered with TiO_2 particles. Experimental conditions: $w = 60$ cm, $L = 120$ cm, initial concentration of oxalic acid $0.01\ \text{mol dm}^{-3}$, $V_r = 15\ \text{dm}^3$, 10 sunbed bulbs at a distance 10.5 cm from the reactor plate, temperature (25 ± 1) °C. Flux of photons 1.13×10^{-8} einstein $\text{cm}^{-2}\ \text{s}^{-1}$. Flow rates, Q: (●) 2.2, (■) 3.5 and (▲) $5.2\ \text{dm}^3\ \text{min}^{-1}$.

The influence of the flow-rate on the degradation of oxalic acid was also investigated. From Fig. 7 and Table 1 it follows that the degradation rate and the photon yield increased with increase in flow-rate. The photon yield was calculated according to Equation 48

$$\Gamma = \frac{v_{hv} V_r}{v_{org} J_{hv} A} \frac{dc_{org}}{d\tau} \times 100 \qquad (48)$$

v_{hv} is the number of photons used for the degradation of v_{org} mole of oxalic acid according to Equation 12, $v_{hv} = 4$, $v_{org} = 2$ for oxalic acid, $dc/d\tau$ is the gradient taken from Figs 7, 10–12 $[\text{mol cm}^{-3}\ \text{s}^{-1}]$, J_{hv} is the average photon flux 1.13×10^{-8} einstein $\text{cm}^{-2}\ \text{s}^{-1}$.

Increase in flow-rate leads to increase in Reynolds number and, of course, to the increase in the thickness of the film circulated over the reactor plate according to Equation 29. The Reynolds number was calculated from Equation 30. The dependence of the film thickness on the film Reynolds number is shown in Fig. 2 for the apparatus used in this study.

4.2.1. Limiting case due to mass transfer. Calculation of the decrease in the oxygen content and oxalic acid content in the flowing part of the liquid film (width 60 cm and length 10 cm) is essential for analysis of limiting cases due to the mass transfer. To calculate the volume of this part of the film (V_{f10}) it is necessary to know the thickness of the liquid film. For given flow rate and inclination angle, Reynolds number (Equation 30) and the average thickness of the liquid film (Equation 29) can be calculated.

Then, the average time (τ_f) for which each molecule in the liquid film is present on the plate can be calculated. First we calculate the average velocity in

Table 1. Oxidation of oxalic acid solutions at the surface of the reactor plate covered by TiO_2 for different flow-rates. Comparison of the experimental and theorectical decomposition rate of the oxalic acid solution

Photon yield was calculated for $\nu_{hv} = 4$. The plate width $w = 60\,\text{cm}$, length $L = 120\,\text{cm}$. $V_r = 15000\,\text{cm}^3, J_{hv} = 1.13 \times 10^{-8}$ einstein $\text{cm}^{-2}\,\text{s}^{-1}$, $c^0_{O_2} = 3.125 \times 10^{-7}\,\text{mol}\,\text{cm}^{-3}$. $D_{O_2} = 2.34 \times 10^{-5}\,\text{cm}^2\,\text{s}^{-1}, D_{(COOH)_2} = 1.169 \times 10^{-5}\,\text{cm}^2\,\text{s}^{-1}$, $\nu_{H_2O} = 0.01\,\text{cm}^2\,\text{s}^{-1}$ [28, 29], temperature $(22 \pm 1)\,^\circ\text{C}$.

Experiment	*Flow-rate* /$\text{dm}^3\,\text{min}^{-1}$	*Initial conc. of oxalic acid* $\times 10^6$ /$\text{mol}\,\text{cm}^{-3}$	(*Experiment*) *Oxalic acid decomp. flux density* $\times 10^{10}$ /$\text{mol}\,\text{cm}^{-2}\,\text{s}^{-1}$	(*Theory*) *Oxalic acid decomp. flux density* $\times 10^{10}$ /$\text{mol}\,\text{cm}^{-2}\,\text{s}^{-1}$	(*Experiment*) *Flux density of oxygen* $\times 10^{10}$ /$\text{mol}\,\text{cm}^{-2}\,\text{s}^{-1}$	*Theoretical limit flux density of oxygen* $\times 10^{10}$ /$\text{mol}\,\text{cm}^{-2}\,\text{s}^{-1}$	(*Experiment*) *Photon yield* /%
1	2.2	9.728	4.775	7.810	2.387	3.905	8.45
2	3.5	9.909	5.729	8.220	2.864	4.110	10.4
3	5.2	10.14	6.898	8.592	3.449	4.296	12.2
4	5.2	10.1	5.692	8.592	2.846	4.296	10.1
5	5.2	4.782	6.679	8.592	3.339	4.296	11.8
6	5.2	2.449	6.925	8.592	3.462	4.296	12.3
7*	5.2	10.43	11.629	12.88	5.814	6.444†	20.6
8*	5.2	4.742	10.543	12.88	5.272	6.444†	18.7
9*	5.2	2.525	9.575	12.88	4.788	6.444†	16.9

* Holding tank bubbled with oxygen.
† Calculated for oxygen concentration $4.69 \times 10^{-7}\,\text{mol}\,\text{cm}^{-3}$.

the film, $\overline{v_f}$ (Equation 31). The time τ_f can be calculated from the following equation:

$$\tau_f = \frac{L}{v_f} \tag{49}$$

The experimental oxalic acid decomposition flux densities are given in Table 1. These values are divided by the area of the part of the liquid film ($600\,\text{cm}^2$) to obtain the decrease in the amount of oxalic acid per time ($\Delta n_{(COOH)_2}/\tau$) in the part of the film due to the photocatalytic decomposition. Multiplying by τ_f gives the decrease in oxalic acid during the flow of liquid film on the plate covered by TiO_2 ($\Delta n_{(COOH)_2}$). Assuming that the photocatalytic degradation of two moles of oxalic acid is connected with the consumption of one mole of oxygen we can also calculate the decrease in the amount of oxygen (Δn_{O_2}).

From the value of the initial concentration of oxalic acid (0.01 and $0.0001\,\text{mol}\,\text{dm}^{-3}$) and oxygen ($3.1 \times 10^{-4}\,\text{mol}\,\text{dm}^{-3}$) in the solution we can calculate the initial amount of oxalic acid ($n^i_{(COOH)_2}$) and oxygen ($n^i_{O_2}$) in the part of the film (V_{f10}). The calculated values are for two flow rates collected in Table 2.

From Table 2 it can be seen that the decay of oxalic acid in the liquid film due to the photocatalytic decomposition for initial concentration ($0.01\,\text{mol}\,\text{dm}^{-3}$) is 0.3% of the initial value. The situation with oxygen is different and the average decay of oxygen in the film is about 9% of the initial amount of oxygen present in the film. The velocity of the film has a parabolic profile which means that the time for which each molecule of oxalic acid and of molecular oxygen in the flowing film is present on the reactor plate is higher near the surface. This causes the highest depletion at the surface of TiO_2 particles.

It is useful to compare the photocatalysis in the flowing film with the theoretical photocatalysis of the solution (the thickness and volume are equal to the thickness and volume of the flowing liquid film) which is present on the horizontal plate covered by TiO_2 particles. During the time for which each molecule of oxalic acid and molecular oxygen in the flowing film are present on the surface of the plate, 9% of the initial amount of molecular oxygen was consumed and a hypothetic surface layer of 63 μm thickness is totally depleted in oxygen.

The results of calculation in Table 2 clearly show that for an initial concentration of oxalic acid $0.01\,\text{mol}\,\text{dm}^{-3}$ the flowing liquid film near the surface of TiO_2 is depleted in oxygen. The flow of the liquid film is laminar and the transport in the film is only by diffusion. For this case of a film reactor there exists a layer along the plate in which the concentration of oxygen changes from zero to the bulk concentration,

Table 2. Calculation of decrease in oxygen content and oxalic acid content in the flowing part of the liquid film (width 60 cm and length 10 cm)

Exp.	Q/$\text{cm}^3\,\text{min}^{-1}$	$c^i_{(COOH)_2}$ /$\text{mol}\,\text{dm}^{-3}$	Re_f	δ_f /mm	V_{f10} /cm^3	v_f /$\text{m}\,\text{s}^{-1}$	τ_f /s	$\Delta n_{(COOH)_2}$ /mol	Δn_{O_2} /mol	$n^i_{(COOH)_2}$ /mol	$n^i_{O_2}$ /mol	*Cons.*† *oxalic acid*/%	*Cons.*† *oxygen* /%
3	5200	0.01	144	0.63	37.8	0.229	5.23	2.165×10^{-6}	1.08×10^{-6}	3.78×10^{-4}	11.7×10^{-6}	0.3	9.2
1	2200	0.01	61	0.47	28.2	0.130	9.23	2.64×10^{-6}	1.32×10^{-6}	2.8×10^{-4}	8.74×10^{-6}	0.9	15.1
–	2200	0.0001	61	0.47	28.2	0.130	9.23	1.28×10^{-7}	0.55×10^{-7}	2.8×10^{-6}	8.74×10^{-6}	4.6	0.6

†consumed oxygen or oxalic acid.

the Nernst diffusion layer. The thickness of this layer increases with the distance from the leading edge of the reactor plate. The thickness of the Nernst diffusion layer along the plate can be calculated from Equation 39; for a flow rate $5.2\,dm^3\,min^{-1}$ ($\delta_f = 630\,\mu m$) this is shown in Fig. 8. Therefore, there exists a diffusion flow of oxygen to the surface of TiO_2 particles which determines the rate of decomposition.

Not every molecule of oxygen which arrives by diffusion at the TiO_2 surface actually undergoes a reaction with trapped electrons and therefore the concentration of oxygen on the surface of TiO_2 cannot be zero. The reality that molecular oxygen, which is transported by diffusion to the surface, is immediately reduced, can be explained by the fact that electrons formed by absorption of u.v. light are, unlike the holes, accumulated on the surface of TiO_2 in the form of Ti^{3+}. A higher number of trapped electrons located on the surface of small particles can lead to an increase of their negative redox potential $E(Ti^{4+}/Ti^{3+})$. The difference in redox potentials of trapped electrons $E\,(Ti^{4+}/Ti^{3+})$ and oxygen $E\,(O_2/O^{2-})$ therefore increases and accelerates the reduction of molecular oxygen. Another reason is due to oxalic acid forming surface complexes on TiO_2 which cause a change in the energy of the trapped electrons. They have a higher negative redox potential and the rate of their reaction with molecular oxygen can increase by several orders of magnitude.

Table 2 shows that for lower initial oxalic acid concentration ($0.0001\,mol\,dm^{-3}$) the decay of oxalic acid in the liquid film due to the photocatalytic decomposition is 4.6% and the decay of oxygen is 0.6%. This means that the liquid film near the surface of TiO_2 is depleted in oxalic acid and the diffusion flow of oxalic acid to the surface of TiO_2 particles determines the rate of oxalic acid decomposition.

Limiting case due to the oxygen diffusion

The theoretical limiting flux for dissolved oxygen was calculated from Equations 40 and 42 and is given in Table 1. The theoretical limiting flux for oxalic acid was calculated from Equations 40 and 42 and, in all cases, it was from five to 40 times higher in comparison with experimentally found fluxes of oxalic acid. This means that for these conditions (concentration of oxalic acid, intensity of the u.v. light) the diffusion of oxalic acid is not the rate determining step.

Experimental oxalic acid decomposition flux density was calculated from the decrease in oxalic acid concentration during photocatalytic degradation. (Equation 14, Table 1.) The experimental oxygen flux density was calculated assuming the fact that the photocatalytic degradation of two moles of oxalic acid is connected with consumption of one mole of oxygen (Equation 16, Table 1). The theoretical oxalic acid decomposition flux density was calculated from the theoretical limiting flux density of oxygen (Equation 16, Table 1).

The effect of the initial concentration of oxalic acid on the degradation rate of oxalic acid was also investigated. That was carried out in experiments 4–6 with free access of oxygen only from the air and in experiments 9–11 with bubbling of pure oxygen into the solution in the trough and the holding tank. Both cases were measured for initial concentrations of 0.01, 0.005 and 0.0025 M of oxalic acid. From Figs 9 and 10 and Table 1 it follows that the degradation rate of oxalic acid and the photon yield are nearly constant for all three initial concentrations and do not depend on the concentration of oxalic acid.

In Fig. 11 the comparison of the experiments with and without bubbling of oxygen is given. From this Figure and Table 1 it follows that the degradation rate and the photon yield are higher for experiments where oxygen was bubbled into the solution. In such experiments the starting concentration of oxygen was higher than the equilibrium oxygen concentration in

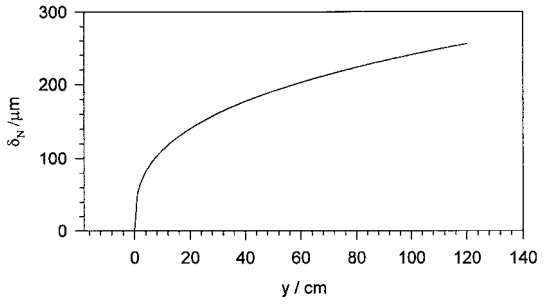

Fig. 8. Thickness of the local Nernst diffusion layer along the length L, $\delta_N(y)$ using Equation 39 for $\nu = 0.01\,cm^2\,s^{-1}$, $\alpha = 10°$, $g = 981\,cm\,s^{-2}$, $D_i = 2.34 \times 10^{-5}\,cm^2\,s^{-1}$, $Q = 5.2\,dm^3\,min^{-1}$.

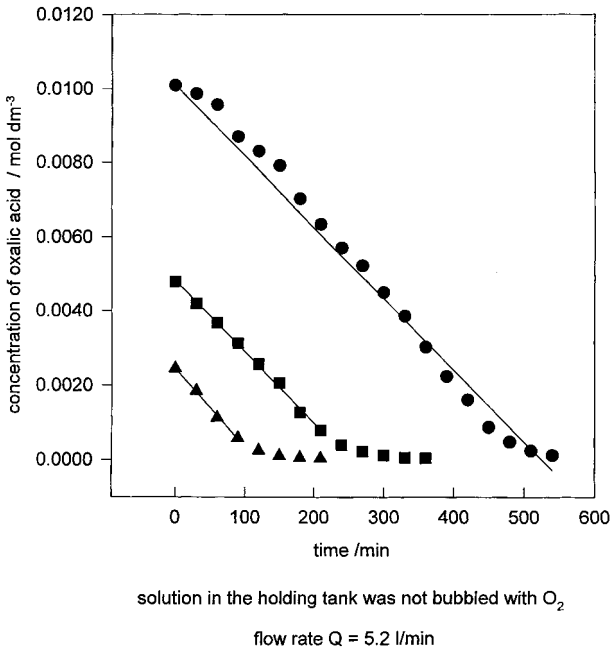

Fig. 9. Concentration of oxalic acid in holding tank against time. Solution in the holding tank was not bubbled with oxygen. $Q = 5.2\,dm^3 min^{-1}$, $V_r = 15\,dm^3$, 10 sunbed bulbs at a distance 10.5 cm from the reactor plate, temperature (23 ± 1) °C. Flux of photons 1.13×10^{-8} einstein $cm^{-2}\,s^{-1}$. $C°$ (initial): (●) 0.0101, (■) 0.004 782 and (▲) 0.002 449 M.

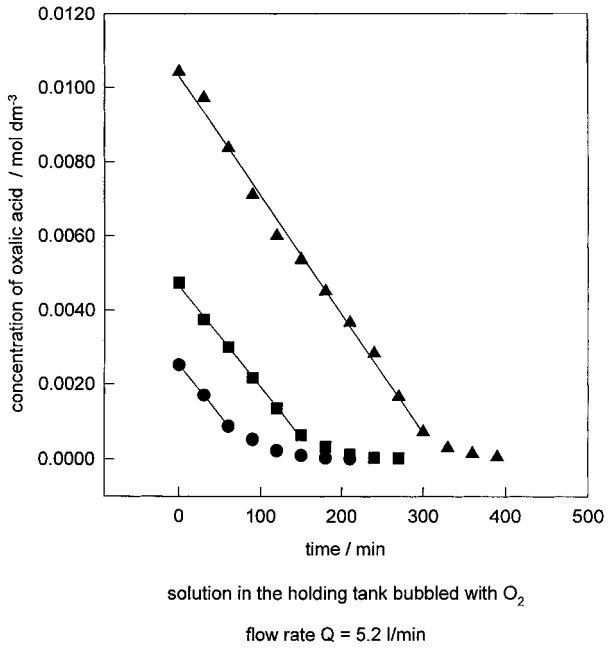

Fig. 10. Concentration of oxalic acid in holding tank against time. Solution in the holding tank was bubbled with pure oxygen. Experimental conditions are the same as in Fig. 9. C° (initial): (▲) 0.0104, (■) 0.004 742 and (●) 0.002 525 M. $Q = 5.2\,\mathrm{dm^3\ min^{-1}}$.

water in contact with air ($3.1 \times 10^{-7}\,\mathrm{mol\,cm^{-3}}$). From [11, 30] it is known that in the presence of suitable electron and hole scavengers the recombination is prevented and a subsequent redox reaction may occur. The authors of [30] established that in experiments with photocatalytic degradation of cyanides, in which oxygen was bubbled through the solution, the cyanide depletion occurred about four times faster than in the air bubbled system, because a higher concentration of the electron scavenger (oxygen) was present for the first case.

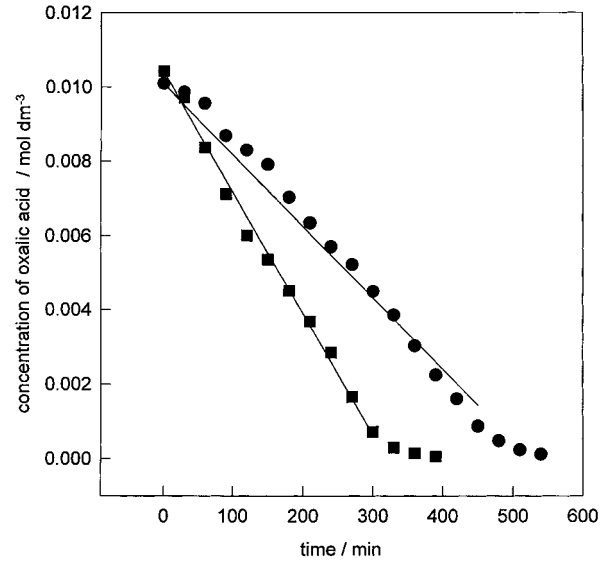

Fig. 11. Comparison of the degradation rate of oxalic acid for experiments with (■, 0.0104 M) and without (●, 0.0101 M) oxygen bubbling into the solution. Experimental conditions are the same as in Fig. 9. $Q = 5.2\,\mathrm{dm^3\ min^{-1}}$.

From thermodynamic calculations it follows that the equilibrium oxygen concentration in dilute aqueous solution in contact with pure oxygen is about $1.5 \times 10^{-6}\,\mathrm{mol\,cm^{-3}}$(22 °C). For experiments with bubbling of oxygen the oxygen concentration was estimated as $4.69 \times 10^{-7}\,\mathrm{mol\,cm^{-3}}$.

4.2.2. Effect of adsorption of oxygen and oxalic acid on TiO_2 surface. Adsorption of reactants can play an important role in the mechanism of photocatalytic degradation of many organic compounds. Initially, the reactant molecules in solution are transferred to the photocatalyst surface and chemically adsorbed; the redox reaction then takes place under irradiation. This process is complex. Under given condition if the rate of oxalic acid decomposition reaction (r_{redox}) is much greater than the rate of reactant diffusion (r_{D}) the reaction will be diffusion-controlled; on the other hand if r_{redox} is much less than r_{D} the reaction can be described by the following Langmuir equation:

$$-\frac{\mathrm{d}c_{\mathrm{org}}}{\mathrm{d}t} = k\Theta(\mathrm{OH}\cdot)^n \tag{50}$$

$$\Theta = \frac{(\mathrm{org})_{\mathrm{ads}}}{S_0} = \frac{c_{\mathrm{org}}}{k + c_{\mathrm{org}}} \tag{51}$$

The Langmuir adsorption isotherm (Equation 50) has been used by many authors to describe the dependence of the degradation rate on the concentration of reactants for various systems but mostly without comparison with a real adsorption isotherm at the same condition. In contrast, Cunningham and Ghassam Al-Sayyed [31] studied adsorption, as well as photocatalytic decomposition, of a derivative of benzoic acid on TiO_2 and concluded that there is no direct connection between the concentration dependence of the photodegradation rate and the adsorption isotherm. This means that the kinetic scheme (Equations 50 and 51) does not include all aspects of the photocatalysis mechanism, even if the dependence of the photodegradation rate on the concentration in the solution formally fulfils the adsorption isotherm.

From Fig. 11 and from Table 1 it follows that the degradation rate of oxalic acid depends on the concentration of oxygen in the solution and its possible adsorption on the TiO_2 surface can be neglected.

4.2.3. Limiting case due to the diffusion of organic compound. The case when the diffusion of the organic compound is limiting is partly shown in Figs 9–11. For the concentration of oxalic acid lower than approximately $0.0003\,\mathrm{mol\,dm^{-3}}$ the decrease in concentration of oxalic acid is slower, the time dependence is exponential and can be described by Equation 28.

The dependence of the logarithm of oxalic acid on time for a very low concentration of oxalic acid, $0.0001\,\mathrm{mol\,dm^{-3}}$, is given in Fig. 12. The other conditions were the same as for experiment 1. The time dependence of oxalic acid concentration in Fig. 12

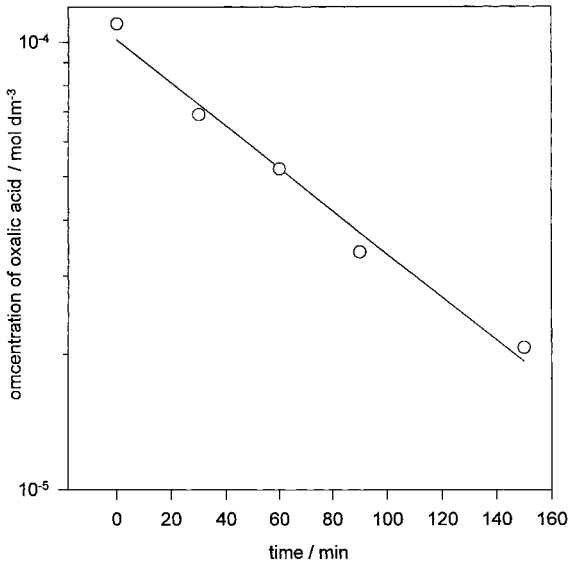

Fig. 12. Logarithm of the concentration of oxalic acid in holding tank against time. The solution in the holding tank was not bubbled with oxygen. $Q = 2.5\,\mathrm{dm^3\,min^{-1}}$, other experimental conditions are the same as in Fig. 9.

may be described by Equation 28. The slope of the curve is $7.99 \times 10^{-5}\,\mathrm{s^{-1}}$ and the theoretical value of the slope $(A\,D_{org})/(V_r\delta_{N,org})$, calculated using Equation 28, is $16.7 \times 10^{-5}\,\mathrm{s^{-1}}$.

From Table 1, it follows, for experiment 1, that to reach agreement between the experimental and theoretical value of the limiting flux of oxygen, the diffusion of oxygen into the porous layer of n-TiO_2 should be accounted for. By approximately doubling the thickness of the Nernst diffusion layer in experiment 1, the theoretical flux density of oxygen is equal to the experimentally found limiting flux density of oxygen (±10%). Also by doubling the theoretically calculated Nernst diffusion layer for the oxalic acid (which means, that the diffusion of oxalic acid into the porous layer of n-TiO_2 is accounted for), the theoretical slope is only $0.5 \times 1.668 \times 10^{-4}\,\mathrm{s^{-1}}$, which is very close to the experimental slope of $7.99 \times 10^{-5}\,\mathrm{s^{-1}}$.

The presented experiments confirmed the theory of limiting cases due to the diffusion of organic compound and oxygen to the surface of TiO_2 particles for the case where the intensity of u.v. light is constant. Further experiments will be performed to confirm the proposed existence of a limiting case due to the light intensity and this will appear in Part II of this paper.

5. Conclusion

Experiments with a model compound, oxalic acid, confirmed the existence of two limiting cases due to the diffusion of oxygen or diffusion of oxalic acid for a photochemical reactor in batch mode. The agreement between theory and experiment was 60–80%. Using additional assumptions about the diffusion of either organic compounds or oxygen into the porous n-TiO_2 layer and for higher flow rates also assuming the influence of waves on the surface of the moving liquid film on the oxygen transfer to the surface of n-TiO_2 layer, a better agreement between the theory and experiment is expected.

Acknowledgement

The authors thank the Grant Agency of the Czech Republic for financial support (grant 203/94/0717) which enabled us to perform this study.

References

[1] Abstracts of the First International Conference on Advanced Oxidation Technologies for Water and Air Treatment, London, Ontario, Canada, 25–30 June (1994).
[2] F. A. DiGiano, *in* 'Control of Organic Substances in Water and Wastewater' (edited by B. B. Berger), Noyes Data Corporation, New Jersey (1987) Chapter 3.
[3] J. J. Rook, *Water Treatment and Examination* **23** (1974) 234.
[4] T. A. Bellar, J. J. Lichtenberg and R. C. Kroner, *J. American Water Works Association* **66** (1974) 703.
[5] J. J. Rook, *Environ. Sci. Tech.* **11** (1977) 478.
[6] R. Rife, T. W. Thomas, D. W. Norberg, R. L. Fournier, F. G. Rinker and M. S. Bonomo, *Environ. Prog.* **8** (1989) 167.
[7] R. B. Pojasek, 'Toxic and Hazardous Waste Disposal', Ann Arbor Science, Ann Arbor, MI (1979), Vols. I–IV.
[8] J. B. Kim, C. S. Gee, J. T. Bandy and C. S. Huang, *J. Water Pollut. Control Fed.* **63** (1991) 501.
[9] H. M. Freedman, 'Incinerating Hazardous Wastes,' Technomic Publishing Co., Lancaster, PA (1988), p. 375.
[10] D. J. De Renzo, *J. Biodegradation Techniques for Industrial Organic Wastes*, Noyes Data Corporation, Park Ridge, NJ (1980), p. 358.
[11] M. R. Hoffman, S. T. Martin, W. Choi, D. W. Bahneman, *Chem. Rev.* **95** (1995) 1.
[12] H. Gerischer, *Electrochim. Acta* **38** (1993) 3.
[13] E. Pellizeti and C. Minero, *ibid.* **38** (1993) 47.
[14] D. Bockelmann, PhD. thesis, 'Photocatalytical Solar Treatment of Waste Water', Technical University Clausthal, Germany (1993).
[15] R. I. Bickley, T. Gonzales-Carreno, J. S. Lees, L. Palmisano and R. J. D. Tilley, *J. Sol. State Chem.* **92** (1991) 178.
[16] S. L. Wilkinson and W. A. Anderson, *in* Abstracts of the First International Conference, op. cit. [1], p. 299.
[17] K. Hashimoto and A. Fujishima, *in* Abstracts of the First International Conference, op. cit. [1], p. 311.
[18] J. F. Kenneke and W. H. Glaze, *in* Proceedings of the Symposium on Water Purification by Photocatalytic, Photoelectrochemical and Electrochemical Processes, The Electrochemical Society, **94** (1994) 365.
[19] D. F. Ollis, E. Pelizzeti and N. Serpone, *in* 'Photocatalytic Fundamentals and Application' (edited by N. Serpone and E. Pelizzeti), Wiley, New York (1989), p. 625.
[20] R. W. Mathews, *J. Phys. Chem.* **91** (1987) 3328.
[21] C. S. Turchi and D. F. Ollis, *J. Phys. Chem.* **92** (1988) 6852.
[22] R. W. Mathews, *ibid.* **92** (1988) 6853.
[23] H. Brauner, 'Grundlagen der Einphasen- und Mehrphasenstroemungen', Verlag Sauerlaender Aarau, Frankfurt/Main (1971), p. 674.
[24] F. Goodridge and G. Gartside, *Trans. Inst. Chem. Eng.* **43** (1965) 62.
[25] I. Roušar, J. Hostomský, V. Cezner, B. Štverák, *J. Electrochem. Soc.* **118** (1971) 881.
[26] K. Javdani, *Chem. Eng. Sci.* **29** (1974) 61.
[27] J. F. Rabek, 'Experimental Methods in Photochemistry and Photophysics', Part II., J. Wiley & Sons, Chichester (1982), p. 947.
[28] G. Houghton, P. D. Ritchi and J. A. Thomson, *Chem. Eng. Sci.* **17** (1962) 221.
[29] Anonymous, 'Physico-chemical Tables,' SNTL, Prague (1953).
[30] C. H. Pollema and J. L. Hendrix, *J. Photochem. Photobiol. A: Chem.* **66** (1992) 235.
[31] J. Cunningham and Ghassam Al-Sayyed, *J. Chem. Soc., Faraday Trans.* **86** (1990) 3935.